CrystEngComm

HIGHLIGHT

View Article Online
View Journal | View Issue

Cite this: *CrystEngComm*, 2025, **27**, 6274

Electrochemistry-induced deposition for controlled formation of metal–organic framework films on insulator and conductor substrates

Takashi Ito * and Elise A. Skinner

A number of technological applications of metal–organic frameworks (MOFs) require the formation of their thin films on insulator and/or conductor substrates at selected areas with desired thicknesses. However, fabrication of such MOF films often requires multi-step processes and/or sophisticated instruments. Herein, we discuss electrochemistry-induced MOF deposition, which permits the direct formation of a thin MOF film with controlled thickness at a desired area on various substrates. So far, we have reported the applicability of this deposition method for the formation of zeolitic imidazolate framework-8 (ZIF-8) films. In this method, a ZIF-8 film is formed on an insulator or a conductor substrate upon applying a cathodic potential to a working electrode that is placed above the substrate. Importantly, the film is formed just below the cathodic working electrode, indicating that the position and lateral dimensions (on the mm- to μm-scale) of the film can be controlled by those of the working electrode. In addition, film thickness is controllable in the range of tens to hundreds of nanometers by adjusting potential application conditions at the cathodic working electrode. These results show that the electrochemistry-induced deposition method will provide a simple means for the fabrication of a patterned MOF film on various substrates without additional lithographic processes.

Received 22nd July 2025,
Accepted 21st August 2025

DOI: 10.1039/d5ce00727e

rsc.li/crystengcomm

Introduction

Metal–organic frameworks (MOFs) are a popular class of crystalline coordination polymers that have garnered attention due to their wide range of potential applications.[1–3] These versatile materials are characterized by nanoscale pores with high effective surface areas leading to their highly ordered self-assembly of metal ions and organic linkers. Furthermore, their crystal structures and associated functions can be fine-tuned through careful selection of metal ions (or clusters) and ligands. The inherent structural properties of MOFs coupled with their tunability have led to the development of MOF materials for gas separation,[4] catalysis,[5,6] energy storage,[7,8] and chemical sensing.[9,10]

Some of these applications have necessitated the development of thin film fabrication methods in order to maximize the utility of the highly ordered nanoporous structure of MOFs.[11,12] Additionally, control of the thickness, area, and position of these films is crucial for use in devices[13,14] such as chemical sensors.[10,15] A variety of methods have been developed to fabricate patterned thin MOF films, including but not limited to MOF growth on prepatterned substrates,[16] contact printing,[17] photolithography,[18–20] inkjet printing,[21,22] and electrochemical deposition.[23,24] One of the earliest methods is the solution-phase formation of a MOF film on prepatterned self-assembled monolayers (SAMs) that are often fabricated *via* microcontact printing.[16] In this method, a MOF film can be preferentially deposited on the surface of a SAM with a terminal functional group that can serve as an anchor for the metal sites of the MOF.[11,16,25] This method permits control of the crystal orientation and film thickness by using a suitable SAM[26] and by adjusting the deposition time,[25] respectively, but is relatively time-consuming because of the initial pattern fabrication and the subsequent slow crystal growth step. Contact printing involves the use of a patterned stamp coated with a precursor solution that is pressed onto a substrate surface and removed upon evaporation of the solvent.[17] This stamp-based method produces MOF films of controlled shapes regardless of substrate terminal groups, but requires relatively long periods of time for crystal growth and affords patterns with limited resolution defined by the feature size and ink spreading. Photolithography stands out from the aforementioned methods as post-synthetic fabrication of a patterned MOF film by removing[18,19] or crosslinking[20] MOFs at selected area(s) *via* photoirradiation. While photolithographic methods offer high-resolution patterning independent of MOF formation, the fabrication process is a time-consuming, multi-step procedure. Inkjet printing yields a film of controlled thickness and shape by

Department of Chemistry, Kansas State University, Manhattan, KS 66506-0401, USA. E-mail: ito@ksu.edu; Fax: +1 785 532 6666; Tel: +1 785 532 1451

spraying a precursor ink from a nozzle onto a flat surface in a precise area.[21,22] While the implementation of affordable office printers makes this method attractive, inks characterized by larger particle sizes or high viscosities can easily clog the narrow nozzle required for high precision patterning and result in low-resolution patterns with undesired defects.[22]

Electrochemical approaches are also examined as a means to form patterned thin MOF films on conductive substrates.[24,27,28] There are three well-established approaches in electrochemical formation of thin MOF films (Fig. 1a–c):[29] anodic deposition (Fig. 1a) is based on oxidative generation of precursor metal ions from the metal electrode,[30] whereas cathodic deposition (Fig. 1b) is controlled by cathodic base generation at the electrode that results in ligand deprotonation to enhance MOF formation.[31,32] Alternatively, electrophoretic deposition (Fig. 1c) utilizes a DC-electric field to attract charged MOF particles to a conductive substrate.[27] In these three approaches, the thickness of a MOF film can be controlled by altering the magnitude and duration of a potential applied to the electrode. Previously, electrochemical formation of patterned MOF films was successfully demonstrated by the use of lithographically prepatterned electrodes[27,28] or by using a microelectrode on a precursor-coated conductive substrate.[24] However, such electrochemical approaches are typically used to form MOF films on an electrically conductive substrate. In addition, these methods were not explored for depositing MOF film(s) at precise area(s) of a non-prepatterned insulator substrate.

In this paper, we discuss an alternative electrochemical approach to the formation of a thin MOF film, electrochemistry-induced deposition (Fig. 1d), which we have recently demonstrated for zeolitic imidazolate framework-8 (ZIF-8).[33,34] In this method, a ZIF-8 film is formed on the surface of a substrate placed underneath a cathodic working electrode: a base generated at the electrode leads to the deprotonation of 2-methylimidazole (Hmim) that enhances the formation of intermediate species composed of Zn^{2+}, Hmim, and mim^{-}. Diffusional accumulation of the intermediate species on the substrate and subsequent crystallization result in the deposition of the ZIF-8 film. Of note, this mechanism is similar to that reported for the deposition of a silica film on a glass substrate using a microdisk electrode.[35] In addition, there were two prior reports on direct MOF deposition on the surface of a non-conductive porous membrane that was induced by the transport of anodic or cathodic products generated at a working electrode across the membrane.[53,54] We will highlight the characteristics of the electrochemistry-induced deposition method and its challenges to be addressed in the future. We believe that the electrochemistry-induced deposition will provide a simple means to fabricate patterned MOF films for various applications, considering its capability to afford a thin MOF film with controlled size/shape and thickness at a desired position on various substrates.

Electrochemistry-induced deposition of ZIF-8 films

We have observed that a thin film can be deposited on the surface of a planar substrate upon applying a cathodic potential to a disk electrode placed above the surface in a methanol solution containing $ZnCl_2$ and Hmim (Fig. 1d).[33] In this method, we use a relatively simple three-electrode cell consisting of a working electrode, a Pt counter electrode, and a Ag/AgCl pseudo-reference electrode. The working electrode is attached to a micrometer for controlling the electrode–substrate distance (Δh) (Fig. 2).

Fig. 3 shows the pictures of thin films that were deposited on (a) a glass substrate,[33] (b) a track-etched polyimide membrane (10 nm in pore diameter, 8 μm thick),[33] (c) a Au-coated Si substrate (Au/Si),[34] and (d) a Si substrate.[34] These pictures clarify the following characteristics of the electrochemistry-induced deposition method. First, this method can be used to deposit a thin film on various substrates regardless of their electrical conductivity, and even on a thin nanoporous polymer membrane. This is because the film deposition is induced by cathodic process(es) at the electrode, not at the underlying substrate. Second, the deposition area can be controlled by the size and position of a working electrode. The diameter of a deposited film is very similar to that of a disk electrode employed and can be as small as tens of microns

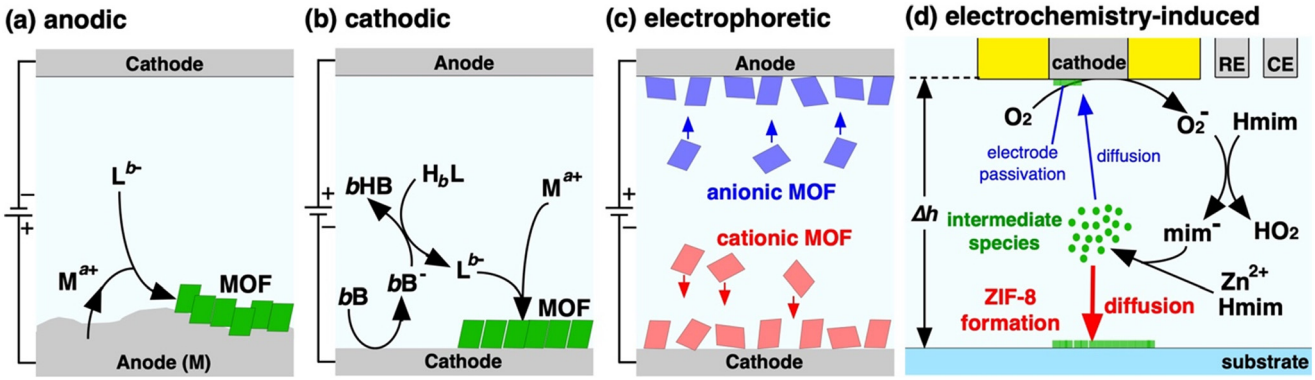

Fig. 1 Schematic illustrations of the formation of a thin MOF film *via* electrochemical processes: (a) anodic deposition, (b) cathodic deposition, (c) electrophoretic deposition, and (d) electrochemistry-induced deposition for ZIF-8. Fig. 1d was adapted with permission from ref. 33. Copyright 2023 American Chemical Society.

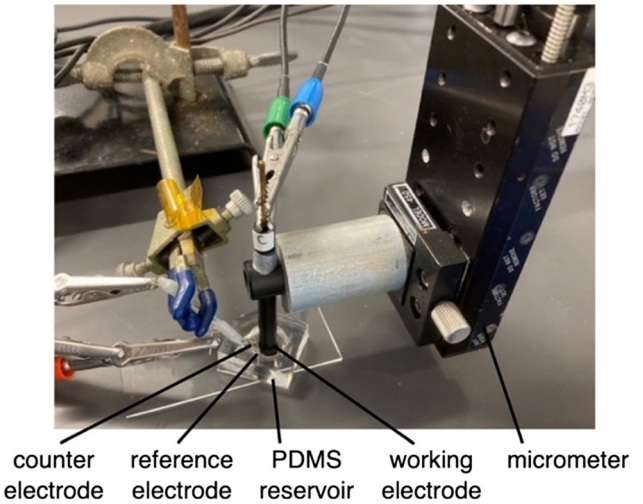

Fig. 2 Experimental setup for the electrochemistry-induced deposition. Adapted with permission from ref. 33. Copyright 2023 American Chemical Society.

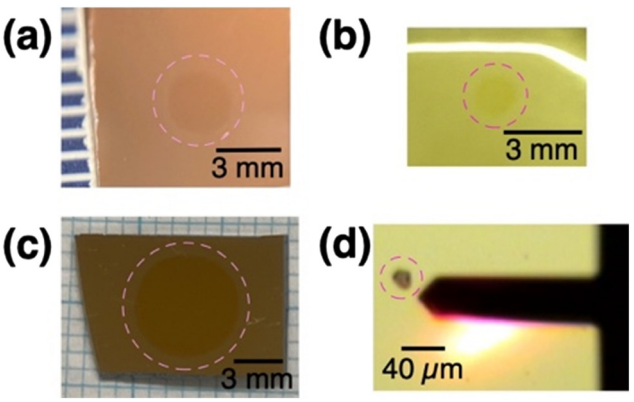

Fig. 3 Pictures of thin films deposited on various substrates using different electrodes in a methanol solution of 10 mM $ZnCl_2$ and 20 mM Hmim at E = −1 V (N = 1): (a) on a glass substrate with a glassy carbon (GC) disk electrode (3 mm in diameter) for 45 min ($\Delta h \approx 150$ μm),[33] (b) on a track-etched polyimide membrane (10 nm in pore diameter, 8 μm thick) with a Pt disk electrode (1.6 mm in diameter) for 15 min ($\Delta h \approx 100$ μm),[33] (c) on a Au-coated Si substrate with a Pt disk electrode (6 mm in diameter) for 15 min ($\Delta h \approx 80$ μm),[34] and (d) on a silicon substrate with a Au ultramicroelectrode (10 μm in diameter) for 15 min ($\Delta h \approx 10$ μm).[34] A deposit has been outlined by a dashed circle. Adapted with permission from ref. 33 and 34. Copyright 2023 American Chemical Society and Copyright 2025 IOP Publishing Limited on behalf of the Electrochemical Society.

using an ultramicroelectrode (Fig. 3d). These results show the possible wide-ranging utility of this electrochemistry-induced method for the fabrication of patterned thin films on various substrates.

The deposited films were ZIF-8, as verified by the X-ray diffraction (XRD) pattern obtained from a film formed on a glass substrate, which showed five peaks corresponding to the (011), (002), (112), (013), and (222) planes of ZIF-8 (Fig. 4a).[33] In addition, XRD peaks from metallic zinc or zinc hydroxides/

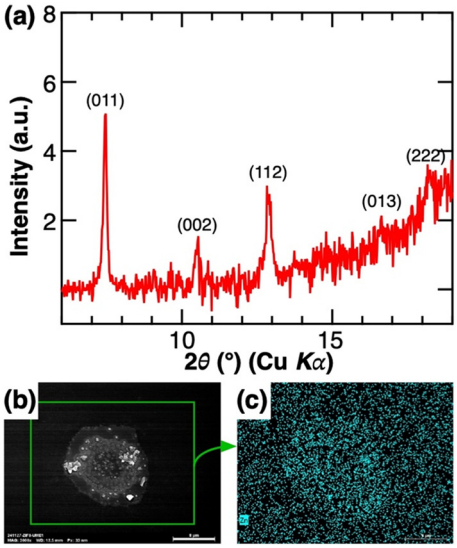

Fig. 4 (a) XRD data of a film (496 nm in ellipsometric thickness) formed on a glass substrate using a Pt disk electrode (6 mm in diameter, Δh = 150 μm) upon five-cycle deposition (N = 5) for t = 30 min.[33] (b) SEM image of a microscale film deposited on a Si substrate using a Au ultramicroelectrode (10 μm in diameter) and (c) its EDX elemental mapping for Zn.[34] Scale bar in (b): 8 μm. Of note, data in Fig. 4b and c were obtained for a film shown in Fig. 3d. Adapted with permission from ref. 33 and 34. Copyright 2023 American Chemical Society and Copyright 2025 IOP Publishing Limited on behalf of the Electrochemical Society.

oxides were not observed.[33] Similar XRD data were obtained for thinner films formed on polyimide sheets using a transmission synchrotron XRD technique.[33] In addition, the distribution of Zn was consistent with the area of a film deposited on a track-etched polyimide membrane[33] and on a Si substrate (Fig. 4b and c).[34]

Selection of precursor solutions, electrode materials, and substrates for the electrochemistry-induced ZIF-8 deposition

As illustrated in Fig. 1d, the following three processes are involved in the electrochemistry-induced ZIF-8 deposition:[33] (1) cathodic generation of a base from O_2 that induces the deprotonation of Hmim to give mim^-;[36] (2) formation of intermediate species composed of Zn^{2+}, mim^-, and Hmim[36–41] underneath the working electrode; (3) diffusional deposition of the intermediate species that leads to ZIF-8 film formation on the underlying substrate. This mechanism implies that the ZIF-8 deposition will be controlled by a number of factors, including the compositions of a precursor solution, electrode materials, the surface properties of underlying substrates, electrode–substrate distance (Δh), applied cathodic potential (E), potential application time (t), and the number of deposition cycles (N).[33,34] Here, we discuss the influences of precursor solutions, electrode materials, and underlying substrates on ZIF-8 film formation, which will provide a guideline for the selection of solutions and materials for the electrochemistry-induced deposition.

(a) Precursor solution. The composition of a precursor solution should give significant influences on the electrochemistry-induced ZIF-8 deposition, because the solution composition controls all three processes, especially the cathodic base generation in process (1) and the formation of intermediate species in process (2). We investigated the effects of Zn^{2+}/Hmim concentration on the ZIF-8 deposition on glass using methanol solutions containing x mM $ZnCl_2$ and $2x$ mM Hmim, *i.e.*, at different stoichiometric concentrations of Zn^{2+} and Hmim.[34] As shown in Fig. 5a, the thickness of a deposited film increased from $x = 0.5$ to $x = 10$, and then reached a plateau (50–60 nm) at the larger x. These observations suggest that the film deposition at $x \leq 10$ and $x \geq 10$ is controlled by the supply of Zn^{2+}/Hmim and a base, respectively. In particular, the plateau at $x \geq 10$ implies that a base primarily involved in the deposition would be O_2^- generated by the reduction of O_2,[36] rather than OH^- generated from H_2O, because the water concentration of the methanol solutions was higher than 10 mM (*ca.* 45 mM H_2O (ref. 34) *vs. ca.* 2 mM O_2 (ref. 42)). On the other hand, larger grains were obtained at the smaller x (Fig. 5b), which would be associated with the slower formation of the intermediate species and a film owing to the limited supply of Zn^{2+}/Hmim. This observation shows a possibility of controlling the surface morphology of a film by changing the Zn^{2+}/Hmim concentrations.

(b) Working electrodes. As shown in Fig. 3, Pt (Fig. 3b and c), Au (Fig. 3d), and glassy carbon (GC) electrodes (Fig. 3a) can be used to deposit ZIF-8 films on various substrates by applying an appropriate cathodic potential (E). The role of the working electrode is to cathodically generate a base (primarily O_2^-, as discussed above) in process (1) that triggers the formation of intermediate species in process (2). Thus, the use of an electrode with higher electrochemical oxygen reduction reaction (ORR) activity should lead to more efficient ZIF-8 deposition on an underlying substrate. Among the three electrodes, the Pt electrode has the highest ORR activity, as shown by the observation of a cathodic current at the most positive potential in a methanol solution containing 10 mM $ZnCl_2$ and 20 mM Hmim (Fig. 6a),[33,34] which was anticipated from prior reports.[43,44] Indeed, a Pt electrode afforded a ZIF-8 film on glass at the more positive E ($E < -0.2$ V) than a GC electrode ($E < -0.5$ V) at the same Δh and t in the methanol solution (Fig. 6b), indicating that a Pt electrode is better suited for the electrochemistry-induced ZIF-8 deposition from the aspect of ORR activity.

In addition, the electrochemistry-induced deposition could be hindered by the passivation of a working electrode (Fig. 1d). Indeed, a working electrode was coated with a film after its use for ZIF-8 deposition on glass (Fig. 6c),[33] which could result from conventional cathodic ZIF-8 electrodeposition (Fig. 1b).[36] The electrode passivation was also realized from a gradual decrease in faradaic current upon multiple potential sweeps in cyclic voltammetry measurements.[33] Importantly, a Pt electrode exhibited smaller cathodic current reduction than a GC electrode (Fig. 6a, dashed lines).[33] The less significant passivation enabled the deposition of a thicker ZIF-8 film on a glass substrate using a Pt electrode (*ca.* 100 nm) as compared with a GC electrode (*ca.* 50 nm) under identical potential application conditions (Fig. 6d).[33] These results indicate that a Pt electrode is optimal as a working electrode for the electrochemistry-induced deposition of ZIF-8 owing to the high ORR activity and the relatively insignificant electrode passivation.

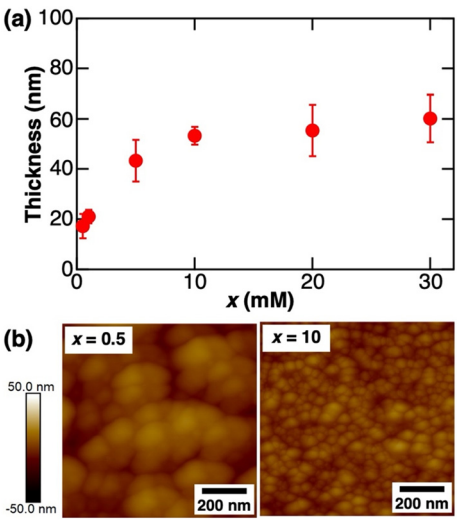

Fig. 5 (a) Effects of $ZnCl_2$/Hmim concentration (x) on the ellipsometric thickness of films deposited on glass using a Pt disk electrode (6 mm in diameter) at $E = -1$ V with $\Delta h = 50$–100 μm for $t = 15$ min ($N = 1$). Of note, films of similar thicknesses were formed in this Δh range, as shown in Fig. 8a. (b) AFM images of films obtained on glass at $x = 0.5$ and 10.[34] Adapted with permission from ref. 34. Copyright 2025 IOP Publishing Limited on behalf of the Electrochemical Society.

(c) Substrate materials

Considering the mechanism shown in Fig. 1d, the electrochemistry-induced deposition should be controlled by the affinity of an underlying substrate to ZIF-8 (and the intermediate species) in process (3). It was also reported that the surface properties of a substrate give significant influences on the deposition kinetics of crystalline materials including MOFs.[12] We thus examined electrochemistry-induced ZIF-8 deposition on planar substrates with different surface properties that were represented by water contact angles ranging from 20° to 110°: Si, glass, and Au/Si substrates in addition to thiolate self-assembled monolayers (SAMs) on Au/Si.[34] Interestingly, we obtained ZIF-8 films of similar thicknesses on these substrates under similar potential application conditions in spite of the large difference in their surface properties (Fig. 7a), revealing the versatility of this method for ZIF-8 deposition on various surfaces. This observation could be associated with their similar surface free energies in the methanol solution, as implied from the similar surface free energies of various SAMs in ethanol.[45,46] On the other hand, ZIF-8 films formed on OH-terminated (and NH_2-terminated) SAMs (OH- and NH_2-SAMs, respectively) consisted

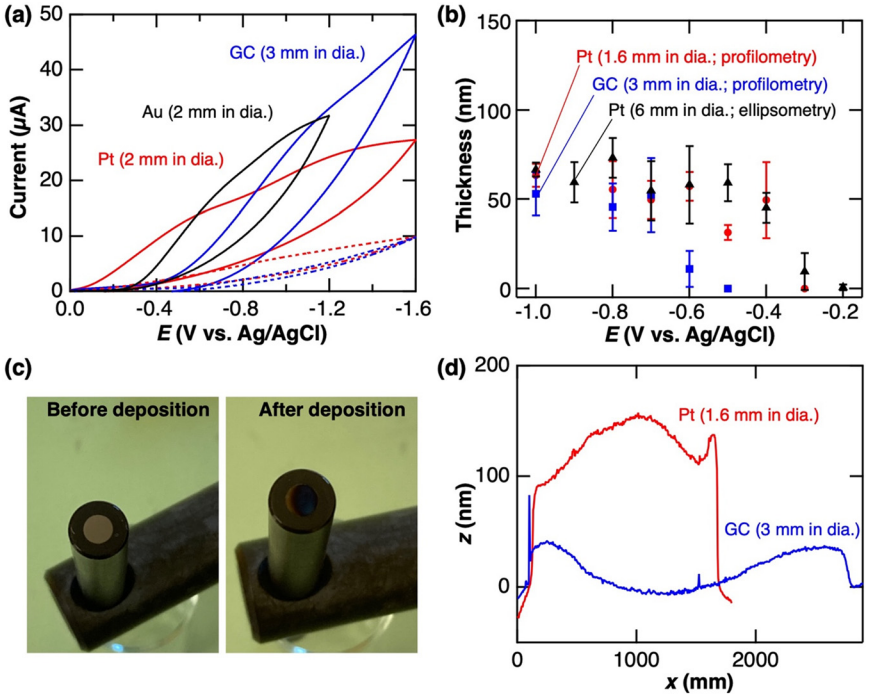

Fig. 6 (a) Cyclic voltammograms (scan rate: 0.1 V s^{-1}) at a Pt disk electrode (2 mm in diameter),[34] a Au disk electrode (2 mm in diameter),[34] and a GC disk electrode (3 mm in diameter).[33] Voltammograms obtained for the first scan and after 11 scans are shown in solid and dashed lines, respectively. (b) Effects of E on the thickness of ZIF-8 films obtained using Pt disk electrodes (1.6 and 6 mm in diameter) and a GC disk electrodes (3 mm in diameter).[33] The films were prepared on glass at $\Delta h \approx 150$ μm, and their thickness was measured using profilometry or spectroscopic ellipsometry. (c) Pictures of a GC disk electrode (3 mm in diameter) before and after being used for ZIF-8 deposition on glass at $E = -1$ V with $\Delta h = 100$ μm for $t = 15$ min.[33] (d) Surface profiles of thin films deposited on glass substrates using Pt and GC disk electrodes (1.6 mm and 3 mm in diameter, respectively) at $E = -1$ V with $h = 150$ μm for $t = 45$ min.[33] All the results shown in Fig. 6 were obtained in a methanol solution containing 10 mM $ZnCl_2$ and 20 mM Hmim. Adapted with permission from ref. 33 and 34. Copyright 2023 American Chemical Society and Copyright 2025 IOP Publishing Limited on behalf of the Electrochemical Society.

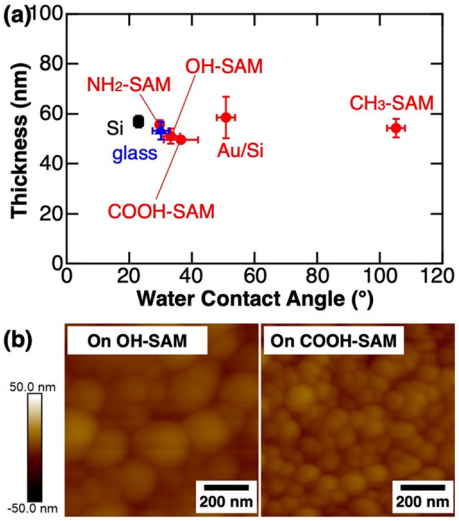

Fig. 7 (a) Thickness of ZIF-8 films formed on different substrates using a Pt electrode (6 mm in diameter) in a methanol solution containing 10 mM $ZnCl_2$ and 20 mM Hmim at $E = -1$ V with $h = 50$–150 μm for $t = 15$ min.[34] (b) AFM images of ZIF-8 films formed on an OH-SAM and a COOH-SAM.[34] Adapted with permission from ref. 34. Copyright 2025 IOP Publishing Limited on behalf of the Electrochemical Society.

of laterally larger grains than those on the other substrates, including a COOH-terminated SAM (COOH-SAM) with similar water contact angle (Fig. 7b). Currently, scientific reasons behind the effects of the surface functional groups on the grain size are unclear, but these results show a possibility of controlling the morphology of a ZIF-8 film based on the surface properties of an underlying substrate.

Control of ZIF-8 film formation by potential application conditions

The mechanism (Fig. 1d)[33] suggests that the electrochemistry-induced ZIF-8 deposition will be influenced by the electrode–substrate distance (Δh) and potential application conditions such as applied cathodic potential (E), potential application time (t), and the number of deposition cycles (N).[33,34] Here, we discuss the effects of these parameters on ZIF-8 film formation, which will permit us to prepare ZIF-8 films with controlled thickness and surface morphology.

(a) Electrode–substrate distance (Δh). The deposition should depend on Δh because of the involvement of the diffusional deposition of the intermediate species on the underlying substrate in process (3) (Fig. 1d). This means that the deposition would be enhanced at the smaller Δh because

the shorter diffusion distance will facilitate attaining supersaturation in proximity to the substrate that is required for the deposition of the intermediate species.[38] As anticipated, thicker films were formed with decreasing Δh at $\Delta h \leq 200$ μm, and the deposition was negligible at $\Delta h \geq 250$ μm (Fig. 8a).[33] On the other hand, deposition at a very small Δh (<10 μm) with a millimeter-scale disk electrode led to the formation of a ring pattern corresponding to the peripheral edge of the electrode, which would reflect the limited supply of Zn^{2+}, Hmim, and O_2.[33] Fig. 8a also shows the greater influence of Δh on the film deposition with a smaller working electrode, as shown by the more consistent increase in film thickness at $\Delta h \leq 100$ μm with the smaller, 1.6 mm diameter electrode. The influence of Δh was more significant when a 10 μm diameter electrode was used: a film could be deposited only at $\Delta h < 20$ μm, indicating that the shorter diffusion distance is required to attain the supersaturation of the intermediate species on the substrate surface owing to the generation of a small amount of O_2^- at the μm-scale electrode.[34] Importantly, Δh could affect the lateral size of a deposited film owing to the diffusion-induced broadening[47] of the distribution of intermediate species, as shown by the microscale ZIF-8 film (Fig. 3d) that had a slightly larger size (*ca.* 16 μm in diameter) than the ultramicroelectrode (10 μm in diameter).[34]

(b) Applied cathodic potential (E)[33]. The cathodic generation of O_2^-, and thus the formation of the intermediate species, can be controlled by E. Indeed, thicker films were obtained at more negative E in the range from −0.2 to −0.6 V for a Pt electrode and from −0.5 to −0.7 V for a GC electrode (Fig. 6b). In these E ranges, the film formation was regulated by cathodic O_2^- generation that was controlled by the ORR kinetics at the working electrode. At the more negative E, the film thickness was independent of E, indicating that the cathodic generation of O_2^- at the working electrode was controlled by the mass transport of O_2 rather than the electrode reaction kinetics. Importantly, E also affected the surface morphology of the film: films consisting of small grains at high density were formed at the plateau range of E (*e.g.*, E = −0.8 V; Fig. 8b, left), whereas isolated larger grains were deposited at the more positive E (*e.g.*, E = −0.5 V; Fig. 8b, right). The formation of the larger grains would be attributed to the slower growth kinetics of the intermediate species that were controlled by the concentration of cathodically generated O_2^-. Of note, isolated grains as shown in Fig. 8b were not observed on films formed at E = −1 V with the lower Zn^{2+}/Hmim concentrations ($x \leq 10$) (Fig. 5b). The difference in film morphology implies that the lower O_2^- and Zn^{2+}/Hmim concentrations afford intermediate species having different structural and/or chemical properties.

(c) Deposition time (t)[33]. The above results suggest a possibility of forming a ZIF-8 film of different thicknesses by varying Δh and/or E. However, adjusting t is a more

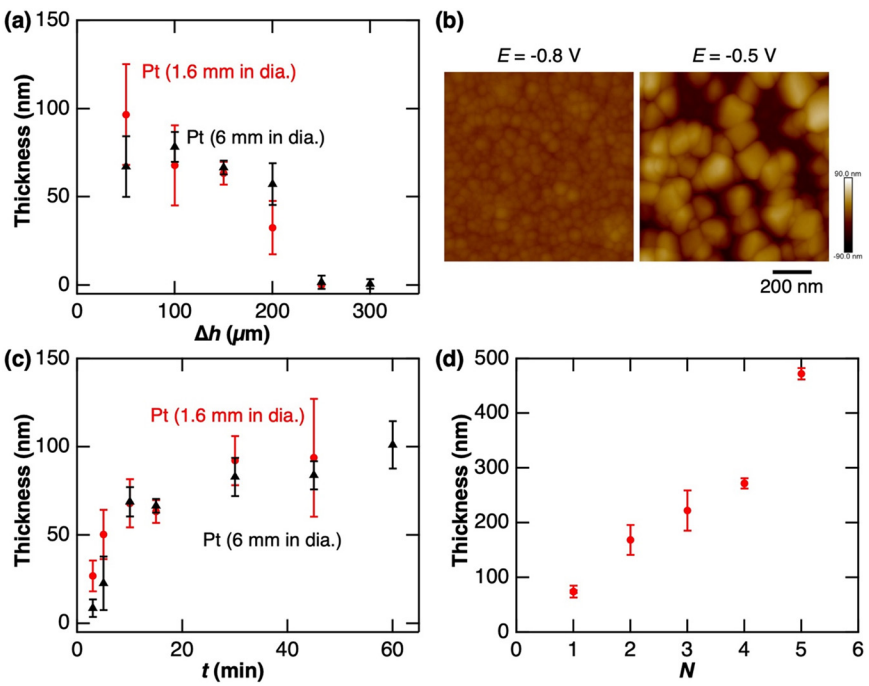

Fig. 8 (a) Effects of Δh on the thickness of ZIF-8 films formed on glass using Pt electrodes (1.6 and 6 mm in diameter) at E = −1 V for t = 15 min (N = 1).[33] (b) AFM images of ZIF-8 films formed on glass at E = −0.8 and −0.5 V using a Pt disk electrode (1.6 mm in diameter) with $\Delta h \approx 150$ μm for t = 15 min (N = 1).[33] (c) Effects of t (N = 1) on the thickness of ZIF-8 films formed on glass using platinum electrodes (1.6 and 6 mm in diameter) at E = −1 V with Δh = 150 μm.[33] Of note, both the electrodes afforded films of similar thickness. (d) Film thickness upon multiple deposition cycles on glass using a platinum electrode (6 mm in diameter) at E = −1 V with Δh = 150 μm for t = 30 min. All the films were formed in a methanol solution containing 10 mM $ZnCl_2$ and 20 mM Hmim, and the thickness of films prepared using 1.6 mm and 6 mm diameter electrodes was measured using profilometry or spectroscopic ellipsometry, respectively. Adapted with permission from ref. 33. Copyright 2023 American Chemical Society.

straightforward way to control film thickness. Fig. 8c shows the thickness of films obtained for different t using platinum disk electrodes (1.6 and 6 mm in diameter) at fixed Δh, E, and N. The film thickness increased from 10 to 100 nm for longer t up to 30 min and reached a plateau thereafter. The former indicates that ZIF-8 films of desired thickness in the range of 10–100 nm can be formed by adjusting t ($\leq$30 min). On the other hand, the plateau observed at $t \geq 30$ min in Fig. 8c shows the limitation of film thickness attainable by single deposition ($N = 1$), which would be attributed to the electrode passivation as discussed above (Fig. 1d and 6c).

(d) Number of deposition cycles (N)[33]. As shown above, the maximum film thickness obtained using a Pt electrode by single deposition ($N = 1$) was *ca.* 100 nm. We could prepare thicker films (>100 nm) *via* multiple deposition cycles ($N > 1$; Fig. 8d) using an unpassivated working electrode, which can be obtained by soaking a working electrode in 0.1 M HCl after each deposition to remove the passivation layer. The film thickness increased proportionally to N, indicating that the multiple deposition cycles provide a means to fabricate ZIF-8 films of hundreds of nanometers and possibly multilayered films composed of different MOFs.

Conclusions

This paper discusses the characteristics of the electrochemistry-induced ZIF-8 deposition approach on insulator and conductor substrates. The deposition is initiated by the cathodic generation of a base (O_2^-) at a working electrode placed above a substrate, followed by the formation of intermediate species that are immobilized *via* diffusion on the substrate to form a ZIF-8 film. This deposition mechanism is consistent with the experimental data, including the effects of the solution composition, electrode material, Δh, and E on the film thickness. Importantly, this method affords a thin ZIF-8 film on a substrate just under a cathodic working electrode, indicating that the position, shape, and lateral dimensions of a film can be controlled by those of a working electrode. In addition, this method provides a means to form ZIF-8 films of controlled thickness in the range of tens to hundreds of nanometers by adjusting the potential application conditions such as t and N. These characteristics indicate the applicability of this method for the direct fabrication of a micropatterned MOF film using a patterned electrode[48] or by scanning a cathodic microelectrode.[24,47,49] Furthermore, this method will be applicable for the patterned deposition of different MOF layers by changing a precursor solution for each of the deposition cycles.

However, there are a number of challenges that limit the utility of this method for such patterned MOF film fabrication. For example, it is currently challenging to form ZIF-8 films of uniform thickness as shown in Fig. 4b and 6d, which would reflect the concentration profiles of the intermediate species during the deposition that would be controlled by the supply of O_2^-, Zn^{2+}, and/or Hmim. The tilting of the surfaces of the working electrode and substrate could also affect the film uniformity. In addition, shorter deposition time (<1 min) is more desirable for scanning probe-based patterning.[47,49] The use of an appropriate probase[28,50] may provide a means to facilitate the electrochemistry-induced deposition. Furthermore, the lateral size of a MOF film may be improved by using a nanoscale electrode with better control of the electrode–substrate distance.[51] Of note, we have reported the electrochemistry-induced deposition only for ZIF-8 so far,[33,34] and are currently examining the applicability of this method for other MOFs. We should point out that fundamental thermodynamic and kinetic research on the formation of intermediate species and crystallization will help overcome these challenges. For example, synchrotron X-ray techniques will permit the *in situ* investigation of electrochemical processes involved in the MOF deposition, which we have recently explored to quantitatively assess the kinetics of cathodic ZIF-8 electrodeposition on graphite electrodes.[52] The resulting in-depth fundamental knowledge will enable the precise control of MOF film deposition on various substrates, and thus the fabrication of micropatterned, multilayered MOF films for various applications such as chemical separation, sensing, and catalysis.

Conflicts of interest

The authors declare no competing financial interest.

Data availability

No primary research results, software or code have been included and no new data were generated or analyzed as part of this highlight article.

Acknowledgements

The authors thank their co-workers for their contributions to the work. This study is partly supported by the Division of Chemical Sciences, Geosciences, and Biosciences, Office of Basic Energy Sciences of the U.S. Department of Energy (DOE) (DE-SC0002362). The work done by TI at the Argonne National Laboratory was supported by the Division of Chemical Sciences, Geosciences, and Biosciences, Office of Basic Energy Sciences of the U.S. DOE under Contract No. DE-AC02-567 06CH11357 and DE-AC02-06CH11357. The National Science Foundation is also thanked for the summer support to EAS (CHE-2305013). This research used resources of the Advanced Photon Source, a U.S. DOE Office of Science User Facility operated for the DOE Office of Science by the Argonne National Laboratory under Contract No. DE-AC02-06CH11357. Experiments at the Center for Nanoscale Materials, a U.S. DOE Office of Science User Facility, were supported by the U.S. DOE, Office of Basic Energy Sciences, under Contract No. DE-AC02-06CH11357.

References

1 S. Kitagawa, R. Kitaura and S.-I. Noro, Functional Porous Coordination Polymers, *Angew. Chem., Int. Ed.*, 2004, **43**, 2334–2375.

2 H.-C. Zhou, J. R. Long and O. M. Yaghi, Introduction to Metal–Organic Frameworks, *Chem. Rev.*, 2012, **112**, 673–674.
3 H. Furukawa, K. E. Cordova, M. O'Keeffe and O. M. Yaghi, The Chemistry and Applications of Metal-Organic Frameworks, *Science*, 2013, **341**, 1230444.
4 Q. Qian, P. A. Asinger, M. J. Lee, G. Han, K. M. Rodriguez, S. Lin, F. M. Benedetti, A. X. Wu, W. S. Chi and Z. P. Smith, MOF-Based Membranes for Gas Separations, *Chem. Rev.*, 2020, **120**, 8161–8266.
5 A. Bavykina, K. Kolobov, I. S. Khan, J. A. Bau, A. Ramirez and J. Gascon, Metal–Organic Frameworks in Heterogeneous Catalysis: Recent Progress, New Trends, and Future Perspectives, *Chem. Rev.*, 2020, **120**, 8468–8535.
6 J. Liu, T. A. Goetjen, Q. Wang, J. G. Knapp, M. C. Wasson, Y. Yang, Z. H. Syed, M. Delferro, J. M. Notestein, O. K. Farha and J. T. Hupp, MOF-Enabled Confinement and Related Effects for Chemical Catalyst Presentation and Utilization, *Chem. Soc. Rev.*, 2022, **51**, 1045–1097.
7 Y. Peng, J. Xu, J. Xu, J. Ma, Y. Bai, S. Cao, S. Zhang and H. Pang, Metal-Organic Framework (MOF) Composites as Promising Materials for Energy Storage Applications, *Adv. Colloid Interface Sci.*, 2022, **307**, 102732.
8 B. He, Q. Zhang, Z. Pan, L. Li, C. Li, Y. Ling, Z. Wang, M. Chen, Z. Wang, Y. Yao, Q. Li, L. Sun, J. Wang and L. Wei, Freestanding Metal–Organic Frameworks and Their Derivatives: An Emerging Platform for Electrochemical Energy Storage and Conversion, *Chem. Rev.*, 2022, **122**, 10087–10125.
9 Y. Zhao, H. Zeng, X.-W. Zhu, W. Lu and D. Li, Metal–Organic Frameworks as Photoluminescent Biosensing Platforms: Mechanisms and Applications, *Chem. Soc. Rev.*, 2021, **50**, 4484–4513.
10 J. E. Ellis, S. E. Crawford and K.-J. Kim, Metal–Organic Framework Thin Films as Versatile Chemical Sensing Materials, *Mater. Adv.*, 2021, **2**, 6169–6196.
11 A. Betard and R. A. Fischer, Organic Framework Thin Films: From Fundamentals to Applications, *Chem. Rev.*, 2012, **112**, 1055–1083.
12 J. Liu and C. Woll, Surface-Supported Metal–Organic Framework Thin Films: Fabrication Methods. Applications, and Challenges, *Chem. Soc. Rev.*, 2017, **46**, 5730–5770.
13 P. Falcaro, R. Ricco, C. M. Doherty, K. Liang, A. J. Hill and M. J. Styles, MOF Positioning Technology and Device Fabrication, *Chem. Soc. Rev.*, 2014, **43**, 5513–5560.
14 C. L. Ruiz-Zambrana, M. Malankowska and J. Coronas, Metal Organic Framework Top-down and Bottom-up Patterning Techniques, *Dalton Trans.*, 2020, **49**, 15139–15148.
15 Q.-J. Sun, W.-T. Guo, S.-Z. Liu, X.-G. Tang, V. A. Roy and X. H. Zhao, Rise of Metal–Organic Frameworks: From Synthesis to E-Skin and Artificial Intelligence, *ACS Appl. Mater. Interfaces*, 2024, **16**, 45830–45860.
16 S. Hermes, F. Schroder, R. Chelmowski, C. Woll and R. A. Fischer, Selective Nucleation and Growth of Metal-Organic Open Framework Thin Films on Patterned COOH/CF_3-Terminated Self-Assembled Monolayers on Au(111), *J. Am. Chem. Soc.*, 2005, **127**, 13744–13745.
17 R. Ameloot, E. Gobechiya, H. Uji-i, J. A. Martens, J. Hofkens, L. Alaerts, B. F. Sels and D. E. De Vos, Direct Patterning of Oriented Metal–Organic Framework Crystals via Control over Crystallization Kinetics in Clear Precursor Solutions, *Adv. Mater.*, 2010, **22**, 2685–2688.
18 G. Lu, O. K. Farha, W. Zhang, F. Huo and J. T. Hupp, Engineering ZIF-8 Thin Films for Hybrid MOF-Based Devices, *Adv. Mater.*, 2012, **24**, 3970–3974.
19 M. Tu, B. Xia, D. E. Kravchenko, M. L. Tietze, A. J. Cruz, I. Stassen, T. Hauffman, J. Teyssandier, S. De Feyter, Z. Wang, R. A. Fischer, B. Marnuroli, H. Amenitsch, A. Torvisco, M. d. J. Velasquez-Hernandez, P. Falcaro and R. Ameloot, Direct X-ray and Electron-Beam Lithography of Halogenated Zeolitic Imidazolate Frameworks, *Nat. Mater.*, 2021, **20**, 93–99.
20 X. Tian, F. Li, Z. Tang, S. Wang, K. Weng, D. Liu, S. Lu, W. Liu, Z. Fu, W. Li, H. Qiu, M. Tu, H. Zhang and J. Li, Crosslinking-Induced Patterning of MOFs by Direct Photo- and Electron-Beam Lithography, *Nat. Commun.*, 2024, **15**, 2920.
21 J.-L. Zhuang, D. Ar, Z.-J. Yu, J.-X. Liu and A. Terfort, Patterned Deposition of Metal-Organic Frameworks onto Plastic, Paper, and Textile Substrates by Inkjet Printing of a Precursor Solution, *Adv. Mater.*, 2013, **25**, 4631–4635.
22 S. A. N. Najafabadi, C. Huang, K. Betlem, T. A. Van Voorthuizen, L. C. P. M. De Smet, M. K. Ghatkesar, M. Van Dongen and M. A. Van der Veen, Advancements in Inkjet Printing of Metal- and Covalent-Organic Frameworks: Process Design and Ink Optimization, *ACS Appl. Mater. Interfaces*, 2025, **17**, 11469–11494.
23 S. Xie, W. Monnens, W. Zhang, W. Guo, N. Han, Z. Zhou, Z. Xue, I. F. J. Vankelecom, X. Zhang and J. Fransaer, Control over Cathodic Deposition of Continuous UiO-66 Films for Ion-Selective Transport, *Cell Rep. Phys. Sci.*, 2023, **4**, 101412.
24 I. Liberman, R. Ifraemov, R. Shimoni and I. Hod, Localized Electrosynthesis and Subsequent Electrochemical Mapping of Catalytically Active Metal–Organic Frameworks, *Adv. Funct. Mater.*, 2022, **32**, 2112517.
25 O. Shekhah, H. Wang, S. Kowarik, F. Schreiber, M. Paulus, M. Tolan, C. Sternemann, F. Evers, D. Zacher, R. A. Fischer and C. Woll, Step-by-Step Route for the Synthesis of Metal–Organic Frameworks, *J. Am. Chem. Soc.*, 2007, **129**, 15118–15119.
26 E. Biemmi, C. Scherb and T. Bein, Oriented Growth of the Metal Organic Framework $Cu_3(BTC)_2(H_2O)_3{\cdot}xH_2O$ Tunable with Functionalized Self-Assembled Monolayers, *J. Am. Chem. Soc.*, 2007, **129**, 8054–8055.
27 I. Hod, W. Bury, D. M. Karlin, P. Denia, C.-W. Kung, M. J. Katz, M. So, B. Klahr, D. Jin, Y.-W. Chung, T. W. Odom, O. K. Farha and J. T. Hupp, Directed Growth of Electroactive Metal-Organic Framework Thin Films Using Electrophoretic Deposition, *Adv. Mater.*, 2014, **26**, 6295–6300.
28 S. Xie, W. Monnens, K. Wan, W. Zhang, W. Guo, M. W. Xu, I. F. J. Vankelecom, X. Zhang and J. Fransaer, Cathodic Electrodeposition of MOF Films Using Hydrogen Peroxide, *Angew. Chem., Int. Ed.*, 2021, **60**, 24950–24957.

29 N. Campagnol, T. R. C. Van Assche, M. Li, L. Stappers, M. Dinca, J. F. M. Denayer, K. Binnemans, D. E. De Vos and J. Fransaer, On the Electrochemical Deposition of Metal–Organic Frameworks, *J. Mater. Chem. A*, 2016, **4**, 3914–3925.
30 R. Ameloot, L. Stappers, J. Fransaer, L. Alaerts, B. F. Sels and D. E. De Vos, Patterned Growth of Metal–Organic Framework Coatings by Electrochemical Synthesis, *Chem. Mater.*, 2009, **21**, 2580–2582.
31 M. Li and M. Dinca, Reductive Electrosynthesis of Crystalline Metal–Organic Frameworks, *J. Am. Chem. Soc.*, 2011, **133**, 12926–12929.
32 S. Xie, Z. Zhou, X. Zhang and J. Fransaer, Cathodic Deposition of MOF Films: Mechanism and Applications, *Chem. Soc. Rev.*, 2023, **52**, 4292–4312.
33 T. Ito, S. G. Jenkins, S. Seifert and A. Uysal, Electrochemistry-Induced Direct Deposition of Nanoscale Thin Zeolitic Imidazolate Framework-8, *Cryst. Growth Des.*, 2023, **23**, 6369–6377.
34 T. Ito and E. A. Skinner, Factors Controlling Electrochemistry-Induced Deposition of a Zeolitic Imidazolate Framework-8 Film on Underlying Substrates, *J. Electrochem. Soc.*, 2025, **172**, 042503.
35 L. Liu, R. Toledano, T. Danieli, J.-Q. Zhang, J.-M. Hu and D. Mandler, Electrochemically Patterning Sol-Gel Structures on Conducting and Insulating Surfaces, *Chem. Commun.*, 2011, **47**, 6909–6911.
36 W. Zhang, Z. Wu, Y. Lv, Y. Li, Y. Zhao, R. Zhang, Y. Xiao, X. Shi, D. Zhang, R. Hua, J. Yao, J. Guo, R. Huang, Y. Cui, Z. Kang, S. Goswami, L. Robison, K. Song, X. Li, Y. Han, L. Chi, O. K. Farha and G. Lu, Oxygen-Assisted Cathodic Deposition of Zeolitic Imidazolate Frameworks with Controlled Thickness, *Angew. Chem., Int. Ed.*, 2019, **58**, 1123–1128.
37 J. Cravillon, C. A. Schroder, R. Nayuk, J. Gummel, K. Huber and M. Wiebcke, Fast Nucleation and Growth of ZIF-8 Nanocrystals Monitored by Time-Resolved In Situ Small-Angle and Wide-Angle X-Ray Scattering, *Angew. Chem., Int. Ed.*, 2011, **50**, 8067–8071.
38 M. J. Van Vleet, T. Weng, X. Li and J. R. Schmidt, In Situ, Time-Resolved, and Mechanistic Studies of Metal–Organic Framework Nucleation and Growth, *Chem. Rev.*, 2018, **118**, 3681–3721.
39 M. W. Terban, D. Banerjee, S. Ghose, B. Medasani, A. Shukla, B. A. Legg, Y. Zhou, Z. Zhu, M. L. Sushko, J. J. De Yoreo, J. Liu, P. K. Thallapally and S. J. L. Billinge, Early Stage Structural Development of Prototypical Zeolitic Imidazolate Framework (ZIF) in Solution, *Nanoscale*, 2018, **10**, 4291–4300.
40 H. H.-M. Yeung, A. F. Sapnik, F. Massingberd-Mundy, M. W. Gaultois, Y. Wu, D. A. X. Fraser, S. Henke, R. Pallach, N. Heidenreich, O. V. Magdysyuk, N. T. Vo and A. L. Goodwin, Control of Metal–Organic Framework Crystallization by Metastable Intermediate Pre-equilibrium Species, *Angew. Chem., Int. Ed.*, 2019, **58**, 566–571.
41 A. R. Dok, S. Radhakrishnan, F. de Jong, E. Becquevort, O. Deschaume, C. V. Chandran, Y. de Coene, C. Bartic, M. Van der Auweraer, W. Thielemans, C. Kirschhock, M. A. van der Veen, T. Verbiest, E. Breynaert and S. Van Cleuvenbergen, Amorphous-to-Crystalline Transformation: How Cluster Aggregation Drives the Multistep Nucleation of ZIF-8, *J. Am. Chem. Soc.*, 2025, **147**, 8455–8466.
42 M. Quaranta, M. Murkovic and I. Klimant, A New Method to Measure Oxygen Solubility in Organic Solvents through Optical Oxygen Sensing, *Analyst*, 2013, **138**, 6243–6245.
43 V. Viswanathan, H. A. Hansen, J. Rossmeisl and J. K. Norskov, Universality in Oxygen Reduction Electrocatalysis on Metal Surfaces, *ACS Catal.*, 2012, **2**, 1654–1660.
44 D. T. Sawyer, A. Sobkowiak and J. L. Roberts, Jr., *Electrochemistry for Chemists*, Wiley, New York, 2nd edn, 1995.
45 A. Noy, C. D. Frisbie, L. F. Rozsnyai, M. S. Wrighton and C. M. Lieber, Chemical Force Microscopy: Exploiting Chemically-Modified Tips to Quantify Adhesion, Friction, and Functional Group Distributions in Molecular Assemblies, *J. Am. Chem. Soc.*, 1995, **117**, 7943–7951.
46 E. W. Van der Vegte and G. Hadziioannou, Scanning Force Microscopy with Chemical Specificity: An Extensive Study of Chemically Specific Tip–Surface Interactions and the Chemical Imaging of Surface Functional Groups, *Langmuir*, 1997, **13**, 4357–4368.
47 D. Mandler and A. J. Bard, A New Approach to the High Resolution Electrodeposition of Metals via the Feedback Mode of the Scanning Electrochemical Microscope, *J. Electrochem. Soc.*, 1990, **137**, 1079–1086.
48 Q.-B. Wu, T. A. Green and S. Roy, Electrodeposition of Microstructures Using a Patterned Anode, *Electrochem. Commun.*, 2011, **13**, 1229–1232.
49 H. Liu, S. Hoeppener and U. S. Schubert, Nanoscale Materials Patterning by Local Electrochemical Lithography, *Adv. Eng. Mater.*, 2016, **18**, 890–902.
50 M. M. Li and M. Dinca, Pt Electrodes Enable the Formation of μ_4-O Centers in MOF-5 from Multiple Oxygen Sources, *ACS Appl. Mater. Interfaces*, 2017, **9**, 33528–33532.
51 J. Clausmeyer and W. Schuhmann, Nanoelectrodes: Applications in Electrocatalysis, Single-Cell Analysis and High-Resolution Electrochemical Imaging, *TrAC, Trends Anal. Chem.*, 2016, **79**, 46–59.
52 T. Ito, S. Seifert, K. N. Moeller and A. Uysal, In Situ Synchrotron X-Ray Scattering Investigation of Cathodic ZIF-8 Deposition on Graphite Using 3D-Printed Cells, *Anal. Chem.*, 2023, **95**, 8206–8213.
53 X. Zhang, Y. Li, C. Van Goethem, K. Wan, W. Zhang, J. Luo, I. F. J. Vankelecom and J. Fransaer, Electrochemically Assisted Interfacial Growth of MOF Membranes, *Matter*, 2019, **1**, 1285–1292.
54 S. Xie, X. Zhang, X. Tan, W. Zhang, W. Guo, N. Han, Z. Zhou, Y. Jiang, I. F. J. Vankelecom and J. Fransaer, One-Step Reductive Electrodeposition of MOF Film on Polymer Membrane, *ACS Mater. Lett.*, 2022, **4**, 1721–1725.

